J Intell Robot Syst (2010) 58:125–147
DOI 10.1007/s10846-009-9347-5

Model Predictive Control of a Flexible Links Mechanism

Paolo Boscariol · Alessandro Gasparetto · Vanni Zanotto

Received: 10 November 2008 / Accepted: 3 June 2009 / Published online: 18 June 2009

Abstract Vibration suppression in flexible link manipulator is a recurring problem in most robotic applications. Solving this problem would allow to increase many times both the operative speed and the accuracy of manipulators. In this paper an innovative controller for flexible-links mechanism based on MPC (Model Predictive Control) with constraints is proposed. So far this kind of controller has been employed almost exclusively for controlling slow processes, like chemical plants, but the authors' aim is to show that this approach can be successfully adapted to plants whose dynamical behavior is both nonlinear and fast changing. The effectiveness of this control system will be compared to the performance obtained with a classical industrial control. The reference mechanism chosen to evaluate the effectiveness of this control strategy is a four-link closed loop planar mechanism laying on the horizontal plane driven by a torque-controlled electric actuator.

Keywords Model predictive control · MPC · Four-link mechanism · Vibration · Constrained optimization

1 Introduction

Model Predictive Control (MPC) refers to a family of control algorithms that compute an optimal control sequence based on the knowledge of the plant and on the feedback information. The dynamic system, together with a set of constraints, is used as the basis of an optimization problem.

MPC is gaining a wider diffusion in different industrial applications, an interesting report about this specific matter can be found in [1]. This kind of control has been

P. Boscariol · A. Gasparetto · V. Zanotto (✉)
DIEGM University of Udine,
via delle Scienze 208, 33100 Udine, Italy
e-mail: vanni.zanotto@uniud.it

first employed in large chemical factories, but in recent years has experienced a wider diffusion to other industrial fields. For examples Chen [2] has recently proposed the use of MPC control in a ball mill grinding process, while Perez [3] deals with control of a rudder roll stabilization control for ships. Other interesting results on MPC control of high-bandwidth systems are [4], [5] and [6].

The availability of more powerful embedded platforms in the last years has encouraged the development of embedded MPC control systems suitable to fast-dynamic plants. For example Hassapis [7] has developed a multicore PC-based embedded MPC control, while FPGA has been chosen by Ling [8] and He [9].

In this paper a model predictive control with constraints is proposed for vibration control in a four-link flexible mechanism. The choice of this control strategy has been motivated by different factors. First, the prediction ability based on an internal model can be a very effective advantage in fast-dynamic systems. Then MPC is well suited to MIMO plants (in this case the mechanical system will be modeled as a SIMO plant), since the outputs are computed by solving a minimization problem which can take account of different variables. Another strong plus of this control strategy is represented by its ability to handle constraints on both control and controlled variables. This can be very effective in real-world control strategies were actuators limitations, such as maximum torque, or maximum speed of motors cannot be neglected. The literature on MPC as an effective vibration reduction strategy in flexible systems is very limited, to authors' knowledge the only paper focusing on this topic is [10], in which a MPC controller is used to control vibrations in a flexible rotating beam through electric motor and piezo-ceramic actuators.

The MPC controller has been implemented in software simulation using Matlab/Simulink™. Exhaustive simulations have been made to prove the accuracy, the effectiveness and the robustness of this control approach. An FPGA implementation of this MPC controller is now being studied, following the results proposed by Ling in [8]. The control system proposed in this paper will be employed to control both the position and the vibration in a four-link flexible mechanism laying on the horizontal plane. The crank is actuated by a torque-controlled electric motor, while the vibration phenomena are measured in the mid-span of the follower link. This work follows a previous work, [11], in which the same authors have experimentally tested the effectiveness of this kind of control system for controlling the position and the vibration in a single-link flexible mechanism. The paper is organized as follows. Sections 2 and 3 explain the mathematical model adopted to simulate the nonlinear dynamic behavior of the overall mechanical system. Since the proposed controller requires a linear state-space model of the controlled system, the linearized model is derived in Section 4, following the procedure traced by Gasparetto in [12]. In the same Section the accuracy of the linearized model is discussed too, together with an evaluation of the performance of the state observer. The Model Predictive Control is briefly presented in Section 5. In Section 6 simulation results obtained controlling the nonlinear system with the MPC controller are presented. The robustness of the controller with respect to the modeling uncertainties is proven in Section 7 by exhaustive simulations, while the effects of choosing different tuning parameters are shown in Section 8. In Section 9 the numerical results of a comparison between the proposed MPC controller and a classical PID controller are presented.

2 Dynamic Model of a Flexible-links Planar Mechanism

In this section the dynamic model of a flexible-link mechanism proposed by Giovagnoni [13] will be briefly explained. The choice of this formulation among the several proposed in the last 30 years has been motivated mainly by the high grade of accuracy provided by this model, which has been proved several times, for example in [14–18]. The main characteristics of this model can be summarized in four points:

- finite-element (FEM) formulation
- equivalent rigid-link system (ERLS) formulation
- mutual dependence of rigid and flexible motion
- suitability to structures with an arbitrary number of both flexible and rigid links

First, each flexible link belonging to the mechanism is divided into finite elements. Referring to Fig. 1 the following vectors, calculated in the global reference frame $\{X, Y, Z\}$, can be defined:

- $\mathbf{r}_i$ and $\mathbf{u}_i$ are the vectors of nodal position and nodal displacement in the ith element of the ERLS and of their elastic displacement
- $\mathbf{p}_i$ is the position of a generic point inside the ith element
- $\mathbf{q}$ is the vector of generalized coordinates of the ERLS

The vectors defined so far are calculated in the global reference frame $\{X, Y, Z\}$. Applying the principle of virtual work, the following relation can be stated:

$$\sum_i \int_{V_i} \delta \mathbf{p}_i{}^T \ddot{\mathbf{p}}_i \rho_i dv + \sum_i \int_{V_i} \delta \epsilon_i{}^T \mathbf{D}_i \epsilon_i dv = \sum_i \int_{V_i} \delta \mathbf{p}_i{}^T \mathbf{g} \rho dv + (\delta \mathbf{u}^T + \delta \mathbf{r}^T)\mathbf{F} \tag{1}$$

Fig. 1 Kinematic definitions

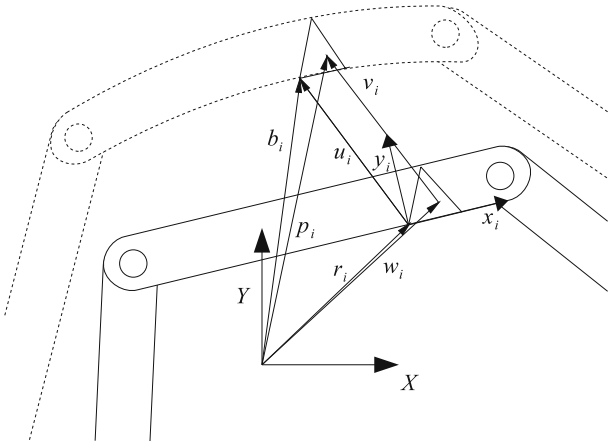

ϵ_i, $\mathbf{D}_i$, ρ_i and $\delta\epsilon_i$ are, respectively, the strain vector, the stress-strain matrix, the mass density of the ith link and the virtual strains. $\mathbf{F}$ is the vector of the external forces, including the gravity, whose acceleration vector is $\mathbf{g}$. Equation 1 shows the virtual works of, respectively, inertia, elastic an external forces. From this equation, $\mathbf{p}_i$ and $\ddot{\mathbf{p}}_i$ for a generic point in the ith element are:

$$\begin{aligned} \delta\mathbf{p}_i &= \mathbf{R}_i\mathbf{N}_i\mathbf{T}_i\delta\mathbf{r}_i \\ \ddot{\mathbf{p}}_i &= \mathbf{R}_i\mathbf{N}_i\mathbf{T}_i + 2(\dot{\mathbf{R}}_i\mathbf{N}_i\mathbf{T}_i + \mathbf{R}_i\mathbf{N}_i\dot{\mathbf{T}}_i)\dot{\mathbf{u}}_i \end{aligned} \tag{2}$$

where $\mathbf{T}_i$ is a matrix that describes the transformation from global-to-local reference frame of the ith element, $\mathbf{R}_i$ is the local-to-global rotation matrix and $\mathbf{N}_i$ is the shape function matrix. Taking $\mathbf{B}_i(x_i, y_i, z_i)$ as the strain-displacement matrix, the following relation holds:

$$\begin{aligned} \epsilon_i &= \mathbf{B}_i\mathbf{T}_i\delta\mathbf{u}_i \\ \delta\epsilon_i &= \mathbf{B}_i\delta\mathbf{T}_i\mathbf{u}_i + \mathbf{B}_i\mathbf{T}_i\delta\mathbf{u}_i \end{aligned} \tag{3}$$

Since nodal elastic virtual displacements ($\delta\mathbf{u}$) and nodal virtual displacements of the ERLS ($\delta\mathbf{r}$) are independent from each other, from the relations reported above the resulting equation describing the motion of the system is:

$$\begin{bmatrix} \mathbf{M} & \mathbf{MS} \\ \mathbf{S}^T\mathbf{M} & \mathbf{S}^T\mathbf{MS} \end{bmatrix} \begin{bmatrix} \ddot{\mathbf{u}} \\ \ddot{\mathbf{q}} \end{bmatrix} = \begin{bmatrix} \mathbf{f} \\ \mathbf{S}^T\mathbf{f} \end{bmatrix} \tag{4}$$

$\mathbf{M}$ is the mass matrix of the whole system and $\mathbf{S}$ is the sensitivity matrix for all the nodes. Vector $\mathbf{f} = \mathbf{f}(\mathbf{u}, \dot{\mathbf{u}}, \mathbf{q}, \dot{\mathbf{q}})$ takes account of all the forces affecting the system, including the gravity force. Adding a Rayleigh damping, right-hand side of Eq. 4 becomes:

$$\begin{aligned} \begin{bmatrix} \mathbf{f} \\ \mathbf{S}^T \end{bmatrix} &= \begin{bmatrix} -2\mathbf{M}_G - \alpha\mathbf{M} - \beta\mathbf{K} & -\mathbf{M}\dot{\mathbf{S}} & -\mathbf{K} \\ \mathbf{S}^T(-2\mathbf{M}_G - \alpha\mathbf{M}) & -\mathbf{S}^T\mathbf{M}\dot{\mathbf{S}} & 0 \end{bmatrix} \begin{bmatrix} \dot{\mathbf{u}} \\ \dot{\mathbf{q}} \\ \mathbf{u} \end{bmatrix} \\ &+ \begin{bmatrix} \mathbf{M} & \mathbf{I} \\ \mathbf{S}^T\mathbf{M} & \mathbf{S}^T \end{bmatrix} \begin{bmatrix} \mathbf{g} \\ \mathbf{F} \end{bmatrix} \end{aligned} \tag{5}$$

Matrix $\mathbf{M}_G$ accounts for the Coriolis contribution, while $\mathbf{K}$ is the stiffness matrix of the whole system. α and β are the two Rayleigh damping coefficients. System in Eqs. 4 and 5 can be made solvable by forcing to zero as many elastic displacement as the generalized coordinates, in this way ERLS position is defined univocally. So removing the displacement forced to zero from Eqs. 4 and 5 gives:

$$\begin{bmatrix} \mathbf{M}_{in} & (\mathbf{MS})_{in} \\ (\mathbf{S}^T\mathbf{M})_{in} & \mathbf{S}^T\mathbf{MS} \end{bmatrix} \begin{bmatrix} \ddot{\mathbf{u}}_{in} \\ \ddot{\mathbf{q}} \end{bmatrix} = \begin{bmatrix} \mathbf{f}_{in} \\ \mathbf{S}^T f \end{bmatrix} \tag{6}$$

In this way, the values of the accelerations can be computed at each step by solving the system in Eq. 6, while the values of velocities and of displacements can be obtained by an appropriate integration scheme (e.g. the Runge-Kutta algorithm). It is important to focus the attention on the size and the rank of the matrices involved, and also to the choice of the general coordinates used in the ERLS definition. Otherwise it might happen that a singular configuration is encountered during the motion of the mechanism. In this case, Eq. 6 cannot be solved.

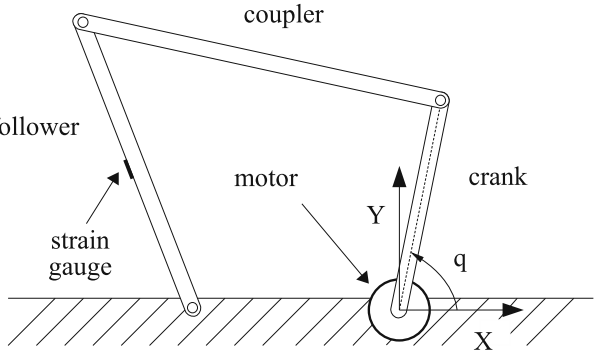

Fig. 2 The four-link mechanism used for simulations

3 Reference Mechanism

The mechanism chosen as the basis of the simulations is a four-link mechanism, made by three steel rods (Fig. 2). The fourth link of the mechanism is the chassis. The section of the rods is square, and their side is 6 mm wide. These three rods are connected in a closed-loop planar chain employing four revolute joints. The first and the third link (counting anticlockwise) are connected to the chassis, which can be considered perfectly rigid. The rotational motion of the first link, which is the shortest one, can be imposed through a torque-controlled actuator. The whole chain can swing along the horizontal plane, so the effects of gravity on both the rigid and elastic motion of the mechanism can be neglected. The length of the links and the

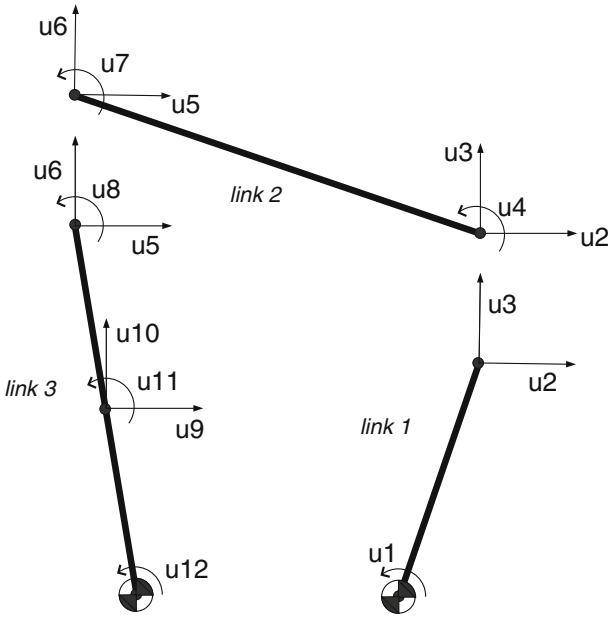

Fig. 3 Elastic displacements in the four-link mechanism

Table 1 Kinematic and dynamic characteristics of reference mechanism

	Symbol	Value
Young's modulus	E	210×10^9 [Pa]
Flexural inertia moment	J	11.102×10^{-10} $[m^4]$
Beams width	a	6×10^{-3} [m]
Beams thickness	b	6×10^{-3} [m]
Mass/unit of length of links	m	272×10^{-3} $[Kg/m]$
Crank length	L_1	0.3728 [m]
Coupler length	L_2	0.525 [m]
Follower length	L_3	0.632 [m]
Ground length	L_4	0.3595 [m]
Rayleigh damping constants	α	8.72×10^{-2} $[s^{-1}]$
	β	2.1×10^{-5} [s]

other geometrical dimensions of the mechanism has been chosen to replicate the actual mechanism prototype (Table 1).

The crank, whose length is $L_1 = 0.3728m$, has been modeled, like the coupler, with a single finite-element (Fig. 3). For the follower, two finite elements have been used, since it is the longer one. Increasing the number of finite elements will certainly improve the overall accuracy of the model, but also includes some drawbacks, in particular it increases the computational effort required for the simulation. Each link described with 1 finite-element has 6 elastic degrees of freedom, whereas the one described by 2 finite-element has 9 degrees of freedom. After putting together the 3 links on the frame, considering the constraints fixed by the kinematic couplings and neglecting one of the nodal displacements in order to make the system solvable (see [13]), the resulting flexible system is described by 12 nodal elastic displacements and one rigid degree of freedom.

4 Linear State-space Dynamic Model

The dynamic model represented by Eq. 6 is strongly nonlinear, due to the quadratic relation between the nodal accelerations and the velocities of the free coordinates. Thus it cannot be used as a prediction model for a linear MPC controller. In order to develop a state-space form linearized version of the dynamic system of Eq. 6 a linearization procedure has been developed by Gasparetto in [12]. Here this procedure will be briefly recalled.

From the basics of system theory, a linear time-invariant model expressed in state-space can be written as:

$$\begin{cases} \dot{\mathbf{x}}(t) = \mathbf{F}_{lin}\mathbf{x}(t) + \mathbf{G}_{lin}\mathbf{v}(t) \\ \mathbf{y}(t) = \mathbf{H}_{lin}\mathbf{x}(t) + \mathbf{D}_{lin}\mathbf{v}(t) \end{cases} \tag{7}$$

where $\mathbf{x}(t)$ is the state vector, $\mathbf{y}(t)$ is the output vector, $\mathbf{v}(t)$ represents the input vector and $\mathbf{F}_{lin}$, $\mathbf{G}_{lin}$, $\mathbf{H}_{lin}$ and $\mathbf{D}_{lin}$ are time-invariant matrices. Taking $\mathbf{x} = [\dot{\mathbf{u}}, \dot{\mathbf{q}}, \mathbf{u}, \mathbf{q}]^T$ as the state vector, linearized state-space form of the dynamic model in Eq. 6 can be written as:

$$\mathcal{A}_{lin}\dot{\mathbf{x}} = \mathcal{B}_{lin}\,\mathbf{x} + \mathcal{C}_{lin}\tau \tag{8}$$

Now a steady "equilibrium" configuration $\mathbf{x}_e$ where $\mathbf{u} = \mathbf{u}_e$ under the system input $\mathbf{v} = \mathbf{v}_e$ can be chosen. In the neighborhood of this point holds:

$$\begin{cases} \mathbf{x}(t) = \mathbf{x}_e + \Delta\mathbf{x}(t) \\ \mathbf{v}(t) = \mathbf{v}_e + \Delta\mathbf{v}(t) \end{cases} \tag{9}$$

Bringing this relations into (6) the following relationship turns out:

$$\mathcal{A}_{lin}(\mathbf{x}_e)\Delta\dot{\mathbf{x}} = \mathcal{B}_{lin}(\mathbf{x}_e + \Delta\mathbf{x})(\mathbf{x}_e + \Delta\mathbf{x}) + \mathcal{C}_{lin}(\mathbf{x}_e + \Delta\mathbf{x})(\mathbf{v}_e + \Delta\mathbf{x}) \tag{10}$$

After some steps that can be found in major detail in [12], $\mathcal{A}_{lin}$ and $\mathcal{B}_{lin}$ matrices in Eq. 8 can be written as:

$$\mathcal{A}_{lin} = \begin{bmatrix} \mathbf{M} & \mathbf{MS} & \mathbf{0} & \mathbf{0} \\ \mathbf{S}^T\mathbf{M} & \mathbf{S}^T\mathbf{MS} & \mathbf{0} & \mathbf{0} \\ \mathbf{0} & \mathbf{0} & \mathbf{I} & \mathbf{0} \\ \mathbf{0} & \mathbf{0} & \mathbf{0} & \mathbf{I} \end{bmatrix} \tag{11}$$

$$\mathcal{B}_{lin} = \begin{bmatrix} -2\mathbf{M}_G - \alpha\mathbf{M} - \beta\mathbf{K} & \mathbf{0} & -\mathbf{K} & 0 \\ \mathbf{S}^T(-2\mathbf{M}_G - \alpha\mathbf{M} - \beta\mathbf{K}) & \mathbf{0} & \mathbf{0} & 0 \\ \mathbf{I} & \mathbf{0} & \mathbf{0} & \mathbf{0} \\ \mathbf{0} & \mathbf{I} & \mathbf{0} & \mathbf{0} \end{bmatrix} \tag{12}$$

$\mathcal{C}_{lin}$ remains unchanged after the linearization process, since it is composed of only zeros and ones. The standard form of the state-space system can be easily found from $\mathcal{A}_{lin}$, $\mathcal{B}_{lin}$ and $\mathcal{C}_{lin}$:

$$\begin{cases} \Delta\dot{\mathbf{x}} = \mathbf{F}_{lin}\Delta\mathbf{x} + \mathbf{G}_{lin}\Delta\mathbf{v} \\ \mathbf{y} = \mathbf{H}_{lin}\mathbf{x} + \mathbf{D}_{lin}\mathbf{v} \end{cases} \tag{13}$$

where:

$$\begin{aligned} \mathbf{F}_{lin} &= \mathcal{A}_{lin}{}^{-1}\mathcal{B}_{lin} \\ \mathbf{G}_{lin} &= \mathcal{A}_{lin}{}^{-1}\mathcal{C}_{lin} \end{aligned} \tag{14}$$

4.1 Accuracy of the Linearized Model

In order to estimate the accuracy of the linearized model, a simple comparison between the impulsive responses for linear and nonlinear models will be set. A more detailed investigation on the accuracy of the linear model can be found on the previous work of the authors [19]. The mechanism will be fed with a 5 Nm torque impulse applied to the crank. The initial configuration has been arbitrarily chosen as $q_0 = 0$ (but the effectiveness of the linearization model holds for any configuration of choice). Here a comparison of the two nodal displacements u_2 and u_{10} is set, but the results extend also to all the other nodal displacements belonging to the model.

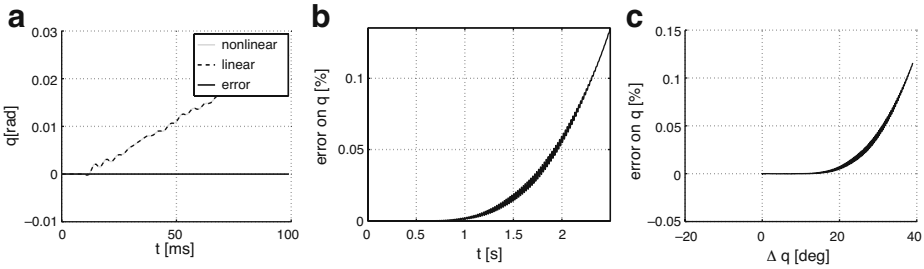

Fig. 4 Crank angular position q. **a** Comparison of the nonlinear and linearized system impulsive responses. **b** Error in per cent vs. time. **c** Error in per cent vs. angular motion from the "equilibrium" configuration

As it can be seen from Fig. 4 the linearized model shows a very high level of accuracy as far as the rigid rotation q is concerned. Figure 4b shows that the error increases as the mechanism moves from the linearization configuration, nevertheless it remains very low. After two seconds of simulation the error between the linear and nonlinear dynamic responses is still lower than 0.1%. Notice that the error reaches the threshold of 0.1% when the crank angular position has moved less or more 40 degrees from the original position (Fig. 4c). The response of the two models show more discrepancies if the nodal elastic displacements u_i are considered. In this situation the kinematic and dynamic nonlinearities affect more heavily the differences between the two responses.

Figure 5 shows the comparison of the nonlinear and linearized system impulsive responses in terms of the nodal displacement u_2. As it can be seen from Fig. 5a the differences are negligible during the transient. Nevertheless they increase as the mechanism moves from the "equilibrium" configuration (Figs. 5b and 5d). In particular the differences on u_2 between the linearized and the nonlinear models are less than the $\pm 20\%$ as long as the motion from the original position is kept less than 80 degrees (Fig. 5c).

A similar behavior can be observed for the all the other displacements. In particular Fig. 6 shows a comparison on the nodal displacement u_{10}. Here the differences between the linearized and the nonlinear models are less than the $\pm 20\%$ as long as the motion from the original position is kept less than 40 degrees (Fig. 6c). This deterioration may be due to the nonlinear effects on the sensitivity matrix $\mathbf{S}(q)$. From the graph in Fig. 5b it can be seen that the absolute linearization error converges to a zero value: it should be stated that this error does not affect the closed-loop control system when it is less than the minimum value that can be measured the acquisition system.

4.2 State Observer

The MPC controller that will be presented and discussed in next sections requires for the whole state vector $\mathbf{x}$ to be available at each sampling time. Nevertheless in practical applications it is impossible to measure all the 12 nodal displacements (and their time derivatives) belonging to the state vector. Hence the need of the

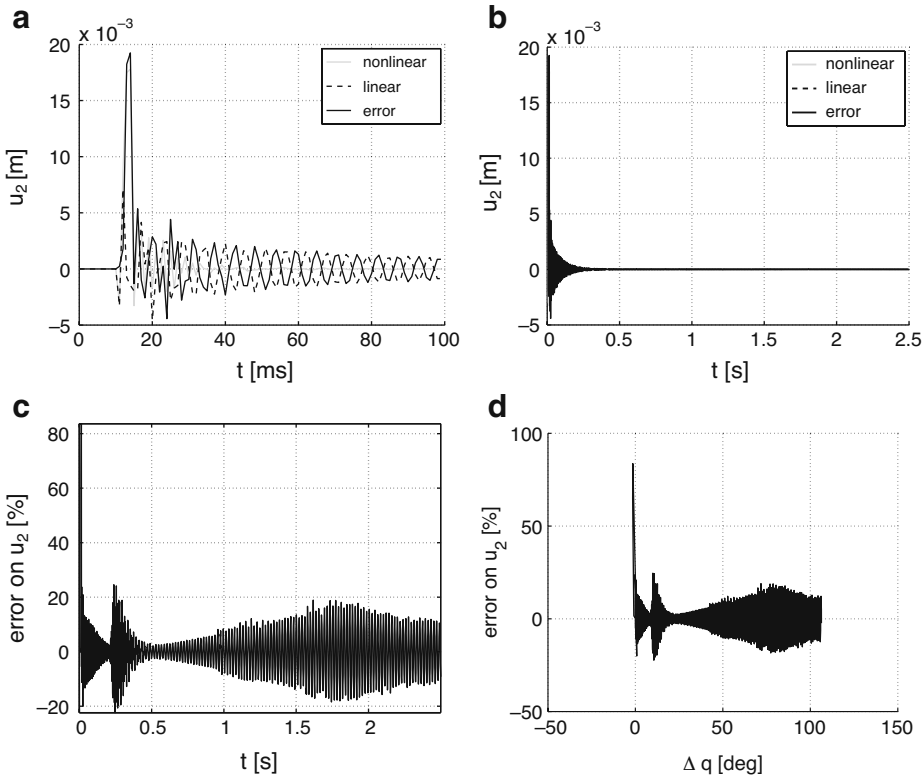

Fig. 5 Comparison of the nonlinear and linearized system impulsive responses for the nodal displacement u_2. **a** Transient responses. **b** Steady state responses. **c** Error in per cent vs. time. **d** Error in per cent vs. angular motion from the "equilibrium" configuration

state observer to obtain an estimate of the full state vector from a subset of it. Here a standard Kalman asymptotic estimator has been chosen. An estimation of $\mathbf{x}(k)$ and $\mathbf{x}_m(k)$ (where $\mathbf{x}(k)$ is the state of the plant model and $\mathbf{x}_m(k)$ is the state of

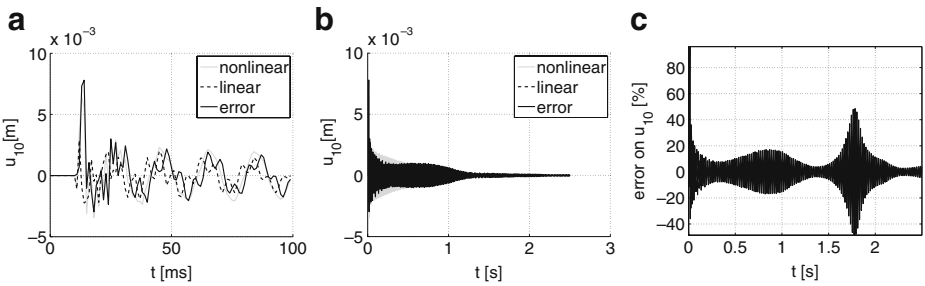

Fig. 6 Nodal displacement u_{10}. **a** Comparison of the nonlinear and linearized system impulsive responses. **b** Absolute error vs. time. **c** Error in per cent vs. angular motion from the "equilibrium" configuration

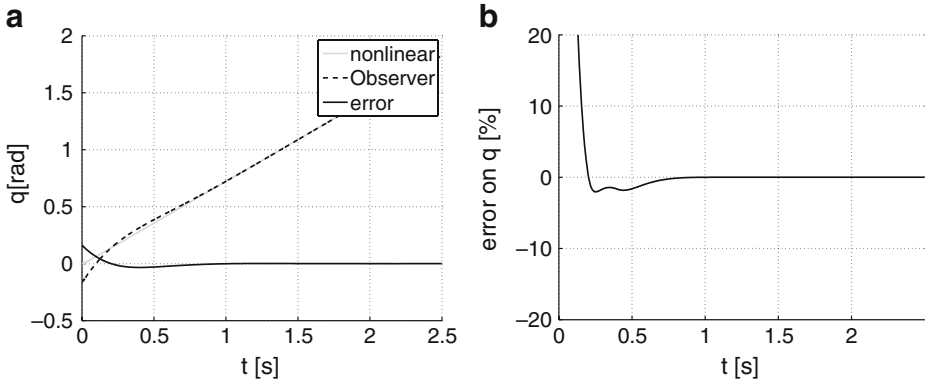

Fig. 7 Displacement q. **a** Comparison of the nonlinear system and observer impulsive responses. **b** Error in per cent vs. time

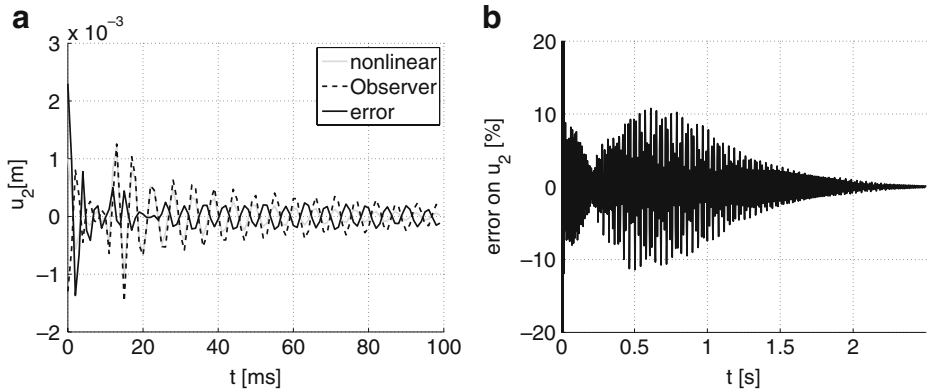

Fig. 8 Nodal displacement u_2. **a** Comparison of the nonlinear system and observer impulsive responses. **b** Error in per cent vs. time

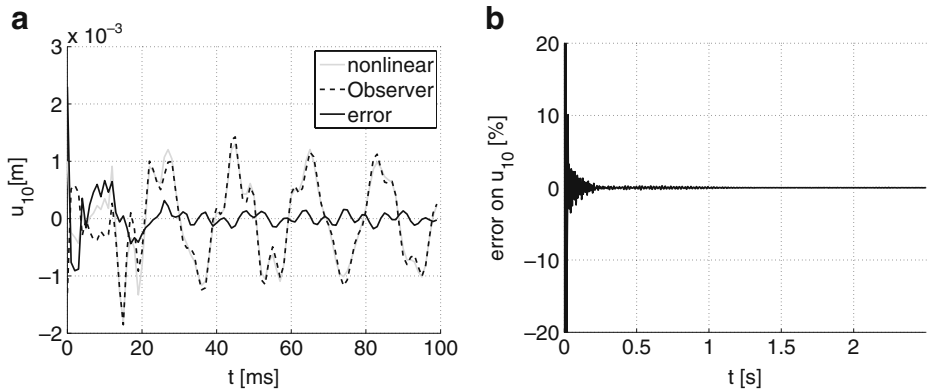

Fig. 9 Nodal displacement u_{10}. **a** Comparison of the nonlinear system and observer impulsive responses. **b** Error in per cent vs. time

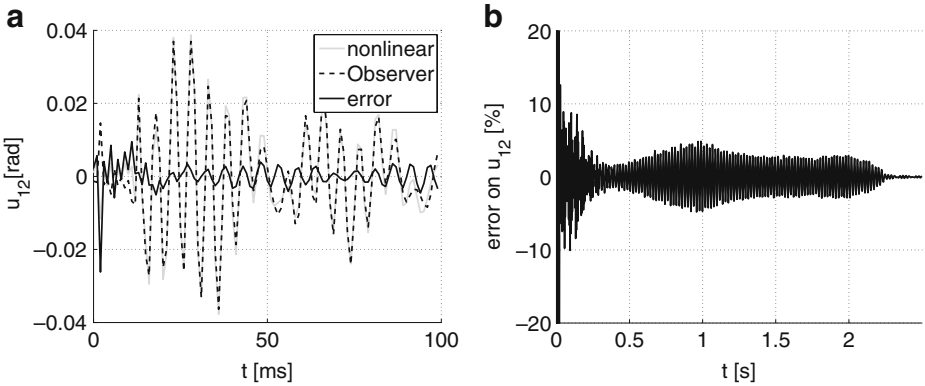

Fig. 10 Nodal displacement u_{12}. **a** Comparison of the nonlinear system and observer impulsive responses. **b** Error in per cent vs. time

the measurement noise model) can be computed from the measured output $\mathbf{y}_m(k)$ trough:

$$\begin{bmatrix} \hat{\mathbf{x}}(k|k) \\ \hat{\mathbf{x}}_m(k|k) \end{bmatrix} = \begin{bmatrix} \hat{\mathbf{x}}(k|k-1) \\ \hat{\mathbf{x}}_m(k|k-1) \end{bmatrix} + \mathbf{M}(\mathbf{y}_m(k) - \hat{\mathbf{y}}_m(k))$$

$$\begin{bmatrix} \hat{\mathbf{x}}(k+1|k) \\ \hat{\mathbf{x}}_m(k+1|k) \end{bmatrix} = \begin{bmatrix} \mathbf{A}\hat{\mathbf{x}}(k|k) + \mathbf{B}_u\mathbf{u}(k) \\ \tilde{\mathbf{A}}\hat{\mathbf{x}}_m(k|k) \end{bmatrix} \tag{15}$$

$$\hat{\mathbf{y}}_m(k) = \mathbf{C}_m\hat{\mathbf{x}}(k|k-1)$$

The gain matrix $\mathbf{M}$ is designed using Kalman filtering techniques, see [20]. Figures demonstrate the effectiveness of the proposed observer, by comparison of

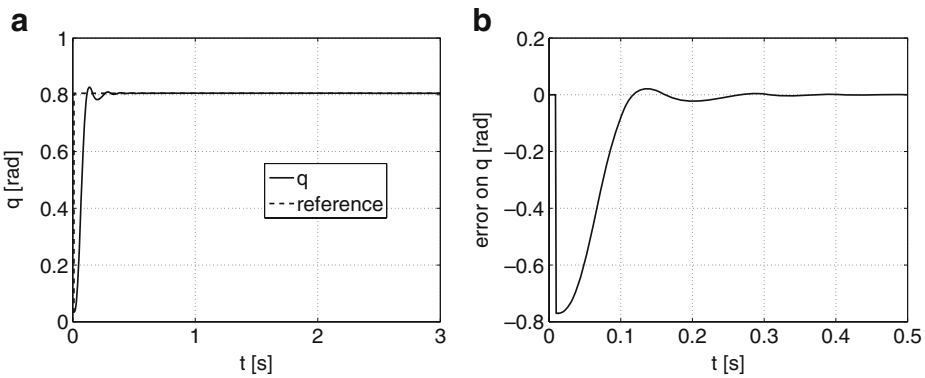

Fig. 11 Angular position of the crank q. **a** Response of the MPC control **b** Error on q

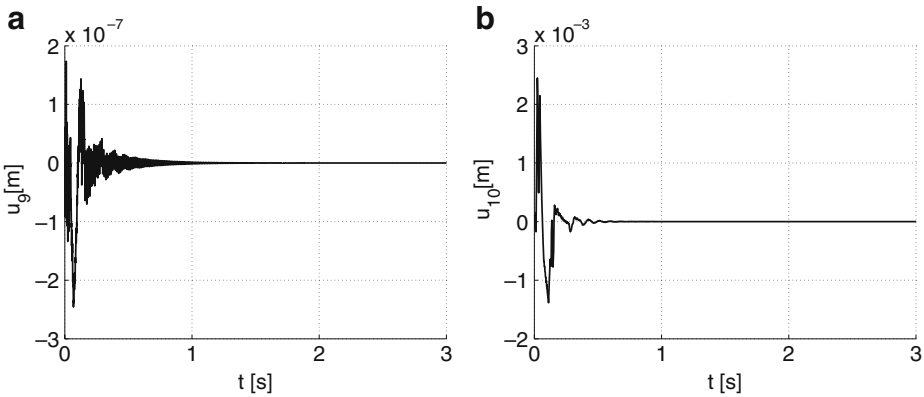

Fig. 12 Elastic displacements measured in the local reference frame employing the MPC control. **a** Elastic displacement u_9 **b** Elastic displacement u_{10}

the impulsive responses of the nonlinear system and the observer. An error on the observer initial state has been assumed, in this way the nonlinear system and the observer started from different initial conditions. In particular each component on the observer initial state vector was different from that of the nonlinear system both in magnitude and in phase: the observer initial condition has been overestimated of 30%, and the sign was changed too. It can be seen that the observer is able both to reduce in few milliseconds the initial error and to keep it below the 10%. Therefor the observer can reproduce with a minimal error the full state vector of the system from the knowledge of u_{10} and q (Figs. 7, 8, 9, 10, 11, and 12).

5 Model Predictive Control with Constraints

In this section the equations leading to the constrained MPC system employed will be briefly analyzed. Basically, MPC control law is calculated as an optimization problem, whose evolution is influenced by both the plant actual input/outputs and its estimated future behavior. In this section a very brief explanation of those concepts is given, for more details see [21].

5.1 Model Prediction

Given a plant model in state-space form:

$$\begin{cases} \mathbf{x}(k+1) = \mathbf{F}\mathbf{x}(k) + \mathbf{G}\mathbf{u}(k) \\ \mathbf{y}(k) = \mathbf{H}\mathbf{x}(k) \end{cases} \tag{16}$$

where $\mathbf{x}(k)$ is the state vector, $\mathbf{y}(k)$ and $\mathbf{u}(k)$ are the vectors of, respectively, outputs and inputs. Assuming that the whole state $\mathbf{x}(k)$ is measured, the future behavior of

the plant at time k over H_p steps, indicated by $[\hat{\mathbf{x}}(k+1|k), \ldots, \hat{\mathbf{x}}(k+H_p|k)]$, can be evaluated as:

$$\begin{aligned}
&\hat{\mathbf{x}}(k+1|k) = \mathbf{F}\mathbf{x}(k) + \mathbf{G}\hat{\mathbf{u}}(k|k) \\
&\hat{\mathbf{x}}(k+2|k) = \mathbf{F}\hat{\mathbf{x}}(k+1|k) + \mathbf{G}\hat{\mathbf{u}}(k+1|k) \\
&\vdots \\
&\hat{\mathbf{x}}(k+H_p|k) = \mathbf{F}\hat{\mathbf{x}}(k+H_p-1|k) + \mathbf{G}\hat{\mathbf{u}}(k+H_p-1|k) = \\
&= \mathbf{F}^{H_p}\mathbf{x}(k) + \mathbf{F}^{H_p-1}\mathbf{G}\hat{\mathbf{u}}(k|k) + \ldots + \mathbf{G}\hat{\mathbf{u}}(k+H_p-1|k)
\end{aligned} \tag{17}$$

Prediction values of outputs are calculated from predicted states:

$$\hat{\mathbf{y}}(k+n|k) = \mathbf{H}\hat{\mathbf{x}}(k+n|k); \qquad n = 1, 2, \ldots, H_p \tag{18}$$

5.2 Constrained Optimization Solution

Supposing to have constraints on both control and controlled variables $u_i(k)$ and z_i(k) respectively, and on their change rate $\Delta u_i(k)$, in terms of linear inequalities, such as:

$$u_{imin} \leq u_i(k) \leq u_{imax} \tag{19}$$

$$\Delta u_{imin} \leq \Delta u_i(k) \leq \Delta u_{imax} \tag{20}$$

$$z_{imin} \leq z_i(k) \leq z_{imax} \tag{21}$$

Those can be expressed as matrix inequalities:

$$\mathbf{V_1}\begin{bmatrix} \mathcal{U}(k) \\ 1 \end{bmatrix} \leq 0 \tag{22}$$

$$\mathbf{V_2}\begin{bmatrix} \Delta\mathcal{U}(k) \\ 1 \end{bmatrix} \leq 0 \tag{23}$$

$$\mathbf{V_3}\begin{bmatrix} \mathcal{Z}(k) \\ 1 \end{bmatrix} \leq 0 \tag{24}$$

$\mathbf{V_1}$, $\mathbf{V_2}$ and $\mathbf{V_3}$ are numeric matrices created to establish a matrix expression, while:

$$\mathcal{U} = \left[\hat{\mathbf{u}}(k|k)^T, \ldots, \hat{\mathbf{u}}(k+H_u-1|k)^T\right]^T$$

is the vector of estimated input values. A similar relation can be used to express also $\Delta\mathcal{U}$. $\mathcal{Z}(k)$ instead can be calculated as in [21]:

$$\mathcal{Z}(k) = \Psi\hat{\mathbf{x}}(k|k) + \Upsilon\mathbf{u}(k-1) + \Theta\Delta\mathcal{U}(k) \tag{25}$$

which results from a different matrix rearrangement of Eq. 17. Without going into further details, Eqs. 23–25 can be putted together in a single inequality:

$$\begin{bmatrix} \Xi \\ \Gamma\Theta \\ \mathbf{W} \end{bmatrix} \Delta\mathcal{U}(k) \leq \begin{bmatrix} -\Xi_i \mathbf{u}(k-1) - \mathbf{f} \\ -\Gamma\left[\Psi\mathbf{x}(k) + \Upsilon\mathbf{u}(k-1)\right] - \mathbf{g} \\ \mathbf{w} \end{bmatrix} \tag{26}$$

where Ξ, Ξ_i and $\mathbf{f}$ are a subset of $\mathbf{V_2}$ such that $\mathbf{V_2} = \left[\Xi, \mathbf{f}\right] = \left[\Xi_i, \ldots, \Xi_{H_p}, \mathbf{f}\right]$, while $\mathbf{V_3}$ can be split as: $\mathbf{V_3} = \left[\Gamma, \mathbf{g}\right]$. $\mathbf{W}$ and $\mathbf{w}$ result from a different formulation of inequality (21), namely:

$$\mathbf{W}\Delta\mathcal{U}(k) \leq \mathbf{w} \tag{27}$$

Once all inequality constraints are collected in a single formula, as in Eq. 27, the focus can be set on the minimization problem, which can be formulated as:

$$\min_{\Delta\mathcal{U}(k)} \Delta\mathcal{U}(k)^T \mathcal{H} \Delta\mathcal{U}(k) - \mathcal{G}^T \Delta\mathcal{U}(k) \tag{28}$$

subject to constraint (27). This minimization problem is a standard QP (quadratic programming) problem, since it is in the form: $\min_{\theta} \frac{1}{2}\theta^T \Phi\theta + \phi^T\theta$ with $\Omega\theta \leq \omega$. Moreover, this problem is convex (see [21]), i.e. there are no local minima that can corrupt its solution.

6 Results of the Model Predictive Controller

In this section the effectiveness of the developed MPC controlled is tested in a simulation environment. This controller acts as a MISO (Multiple-Input, Single-Output) system: the MPC relies on the knowledge of the instantaneous values of the displacements u_{10} and crank angular position q. u_{10} and q are the two controlled variables, while the torque applied to the crank acts as the control variable. The tuning of the MPC depends on 5 variables:

1. weight on u_{10}: w_{10}
2. weight on q: w_q
3. sampling time: T_s
4. prediction horizon: H_p
5. control horizon: H_c

Then constraints on both control and controlled variables should to be taken into account. Here inequalities constraints have been used:

1. $u_{10_{min}} \leq u_{10} \leq u_{10_{max}}$
2. $q_{min} \leq q \leq q_{max}$
3. $\tau_{min} \leq \tau \leq \tau_{max}$

The overall behavior of the controller depends on a large set of variables. While τ_{min} and τ_{max} depends on actuator peak torque, all the others parameters can be tuned quite freely. As a simple rule of thumb, the inequalities constraints should be chosen thinking about the desired performance of the closed-loop system, but always taking care of not setting them too tight, otherwise the system may behave unexpectedly.

Values of T_s, H_p and H_c should, in practical applications, be chosen according to the available computational resources. Every choice of T_s requires to solve the optimization problem $1/T_s$ times every second, and the computational cost of every evaluation is directly proportional to both H_p and H_c.

Referring to [8], Ling proved that a 1.5 million gates FPGA can handle values of T_s around 20 ms without using particular optimization strategies and high-level FPGA programming (the dynamic system size was 2, $T_s = 20ms$, $H_c = 3$, $H_p = 10$). On the other side, Bleris in [4] proved that using more specialized hardware and optimization techniques allows to set T_s as low as 1 ms (the size of the dynamic system was 4, $H_c = 3$, $H_p = 10$).

The model obtained from linearization (evaluated on the initial configuration of the mechanism) will be used to develop the MPC linear controller. Then the MPC will be employed to control the position of the nonlinear mechanism, keeping as small as possible the deformations during the overall motion. The tuning of the MPC controller is chosen to be: $T_s = 1$ ms, $H_p = 55$ and $H_c = 5$. By using these values very high performances can be obtained both in terms of the crank angular position tracking and of the vibrations damping. The final angular position is reached in a very short time (more or less 100 ms), while the elastic displacements reaches a negligible level after less than 500 ms.

In Fig. 13 the mechanism is show at $t = 0$, in $t = 0.120$ s and in $t = 1$ s, hence respectively before the motion, during the transient, and when the mechanism is steady at its final configuration. The elastic displacements, calculated using some interpolation functions, are amplified 10 times in order to make links deformation more evident. As it can be seen in Fig. 13, the largest displacements are the located

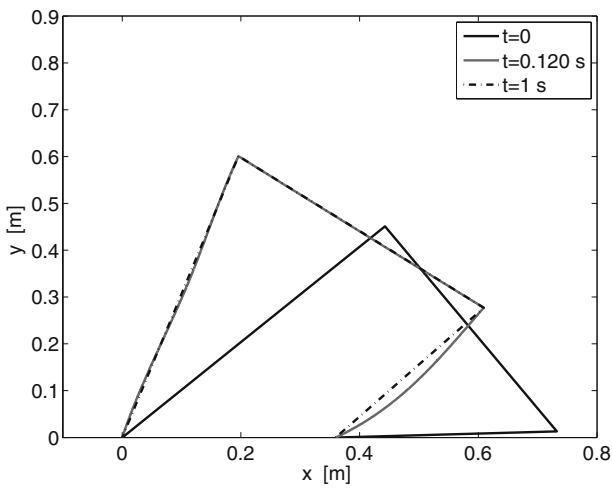

Fig. 13 Mechanism configurations: initial, during the motion, final. Elastic deformation is displayed with a $\times 10$ gain

along the crank, while the vibration along the follower are kept small by the control action.

7 Robustness

In order to verify the robustness of the proposed control scheme, exhaustive tests have been made. A set of simulations have been made employing the same control system on different perturbed nonlinear model. The purpose of these perturbation is to mimic the effects of uncertainties in the model. A great deal of experimental tests have been made with uncertainties of different sign (i.e. +20%, −20%) on the parameters that mostly influence the response of the nonlinear model, such as the value of the length of the first link L_1, the linear mass density m of the links, the elastic modulus E. Moreover, further tests have been made by altering the accuracy of the torque provided by the closed-loop control system: in this way the torque fed to the motor differs to both the optimal torque value computed by the MPC controller and the torque used by the state observer to estimate the actual state of the plant. This approach to robustness analysis has been used in other works, such as [22], where different non-nominal plant are employed to show the capabilities of the proposed control over a classical one by the means of software simulation tests.

In Fig. 14 the effects of altering the linear mass density m of all the links belonging to the mechanism are tested. As it can be clearly seen, an underestimation of the linear mass density by the controller does not bring the closed loop to an unstable behavior: when the actual mass of the links is 30% more than the nominal case the response of the system gets more damped. The same variation in the other direction (−30%) of the m parameter does not lead to instability, as it just increases the overshoot of the angular position tracking. In the two perturbed cases the influence on the vibration damping is quite subtle, especially when the transient is over.

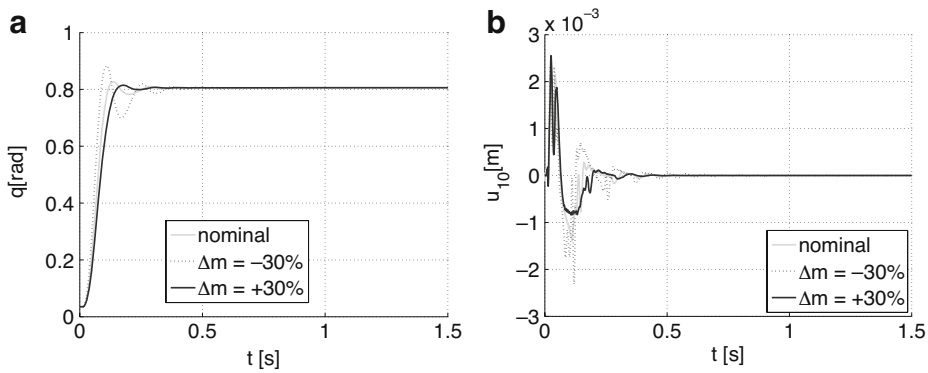

Fig. 14 Robustness analysis to the change of linear mass density m. **a** Angular position q. **b** Elastic displacement u_{10} measured in the local reference frame

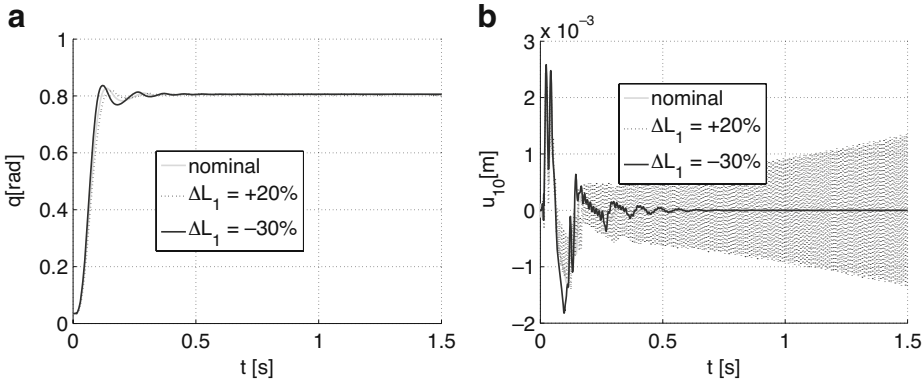

Fig. 15 Robustness analysis to the change of length of the first link L_1 **a** Angular position q. **b** Elastic displacement u_{10} measured in the local reference frame

The change to the parameter L_1, which represents the length of the first link, can be harmful to the stability of the closed-loop system, as can be seen in Fig. 15. A 30% overestimation of the parameter L_1 has little or no effects on the response of the system: in this case the evolution of variables q and u_{10} are the same as the nominal plant's one. In case of a 20% underestimation of L_1 (here the actual length of the link is 20% longer than the same link of the modeled plant) the closed-loop system is no more stable: the evolution of the values represented in Fig. 15 resembles the evolution of an unstable plant.

The closed-loop system retains its performance even in presence of a mismatch between the actual and the estimated elasticity of the links, which is represented by the means of the elastic modulus E. In Fig. 16 it can be seen that altering this value

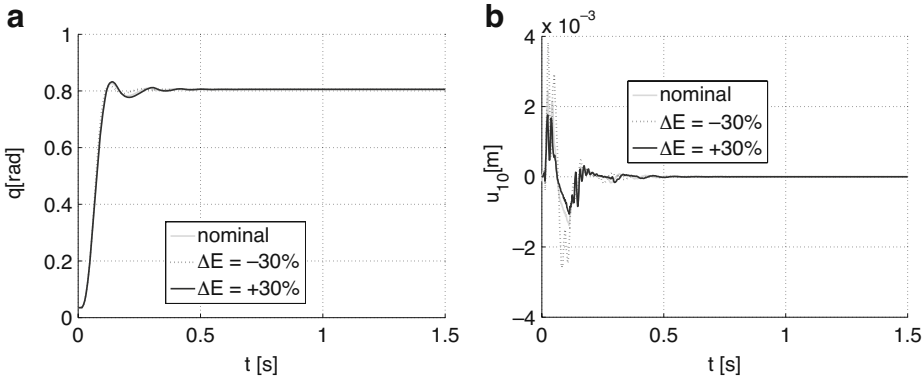

Fig. 16 Robustness analysis to the change of elastic modulus E **a** Angular position q. **b** Elastic displacement u_{10} measured in the local reference frame

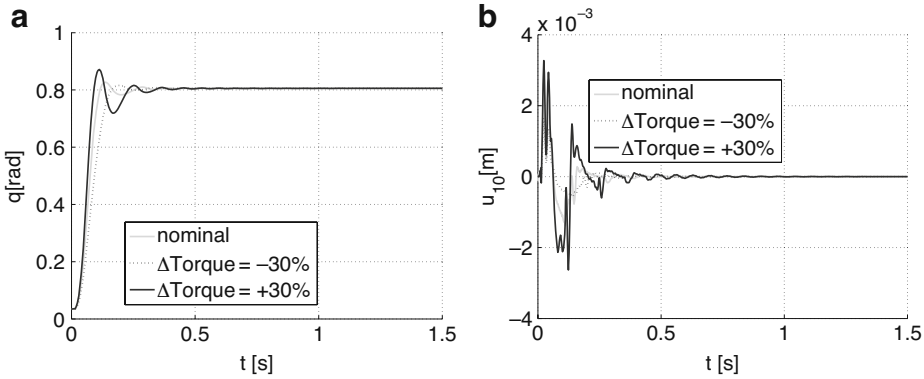

Fig. 17 Robustness analysis to the change of applied torque: **a** Angular position q. **b** Elastic displacement u_{10} measured in the local reference frame

of a $\pm$ 30% factor does not affect the performance of the control system: this means that the proposed controller is robust to a change of the vibration modes of the plant.

In Fig. 17 the effects of a gain error in the estimation of the applied torque is tested. As can be seen in Fig. 17 the performance of the closed-loop system are almost not affected by a $\pm$30% factor. In case of an overestimation of the applied torque (the actuator provides less torque than the desired one) the response of the system is slower. When the torque is underestimated by the observer and by the control system, the closed-loop response has more overshoot but the plant remains stable.

In Fig. 18 the results of three tests are displayed in the same graphs: the nominal plant is first controlled with the nominal torque, then a +30% gain error is introduced,

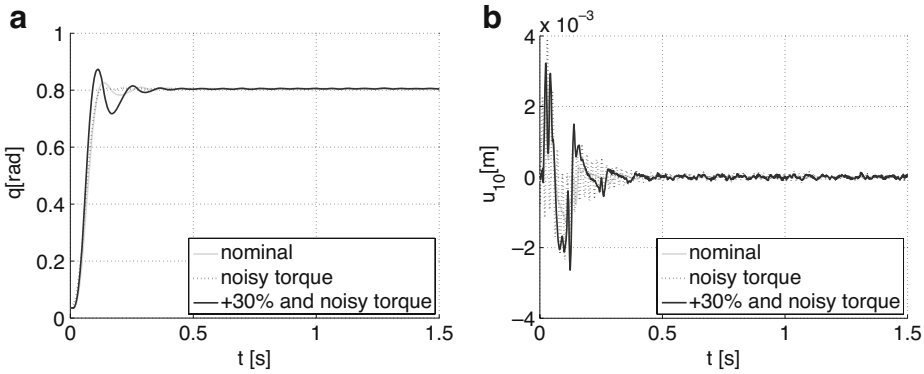

Fig. 18 Robustness analysis to the change of applied torque and noisy torque: **a** Angular position q. **b** Elastic displacement u_{10} measured in the local reference frame

then also an additive white gaussian noise is added to the torque. Again, the MPC controller shows its robust behavior: even when noise is added the response of the system has just a small degradation of the performances.

8 Effects of H_c, H_p and f_c on the Closed-loop System

In this section the effects of choosing different values for the tuning parameters of the MPC controlled are investigated by the means of simulation tests. In Fig. 19 the effectiveness of the controller is evaluated for different values of the sampling frequency of the control system, in order to test the effects of less computational power demanding control systems. It can be seen that the performance of the system are less satisfactory for $f_c = 100$ Hz. This performance reduction might be due to the the lesser efficacy of the system observer at lower frequency, since this has been tuned for a 1 ms refresh time.

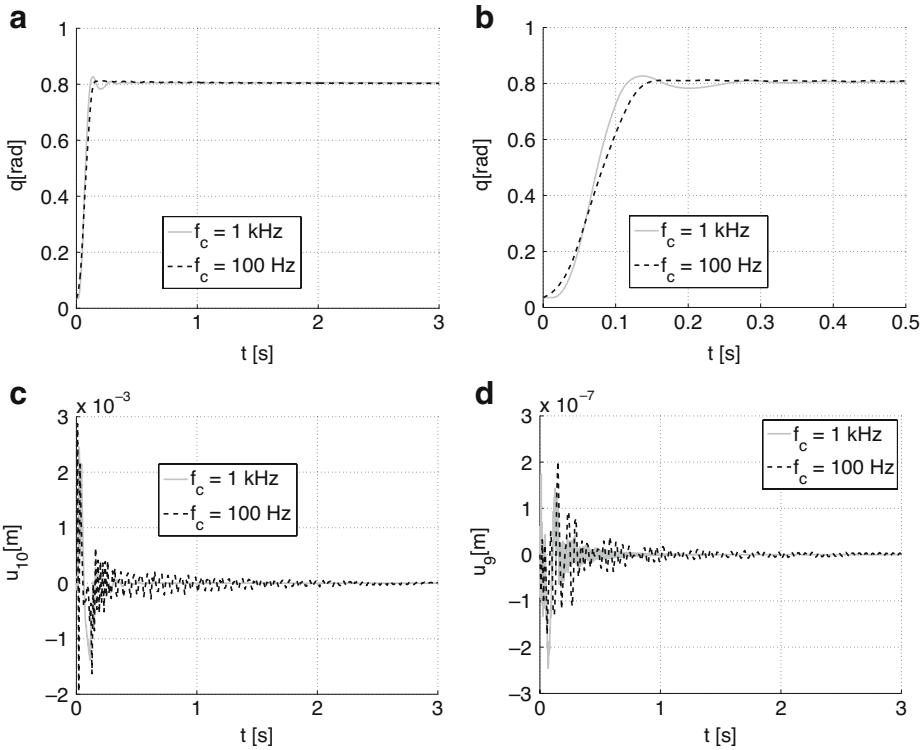

Fig. 19 Response of the control system at with different sampling frequency: 1 kHz and 100 Hz **a** Angular position q. **b** Angular position q: zoom view **c** Elastic displacement u_{10} measured in the local reference frame **d** Elastic displacement u_9 measured in the local reference frame

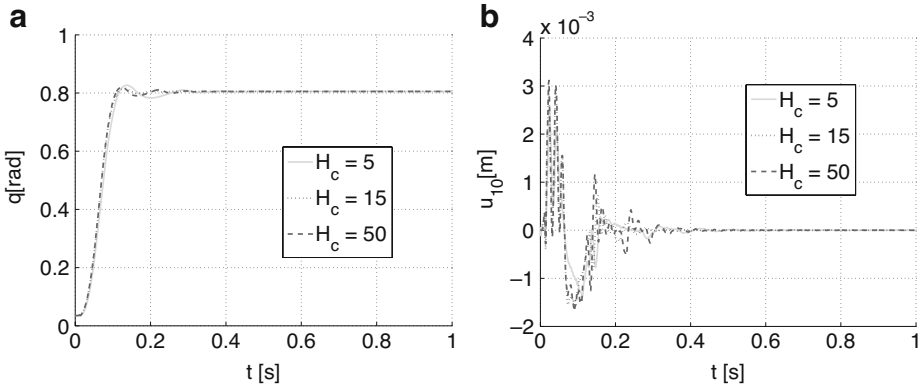

Fig. 20 Analysis of the effects of different control horizon H_c: **a** Angular position q. **b** Elastic displacement u_{10} measured in the local reference frame

In Fig. 20 the effects of choosing different control horizon is investigated: it can be seen that this tuning parameter has a limited effect on the response of the closed-loop system. In particular reducing the control horizon H_p to 5 introduces a small degradation of the performances: the overshoot is slightly increased and the transient response is a little slower. H_c can be increased up to the length of the prediction horizon (here $H_p = 55$) but this choice does not improve the performances of the controller. In practical situations H_c should be kept quite small, since a longer control horizon increases the computational weight of the minimization problem solved by the MPC controller.

Changing the length of the prediction horizon H_p has little or no effects on the performance of the controller when dealing with a nominal plant, since it affects

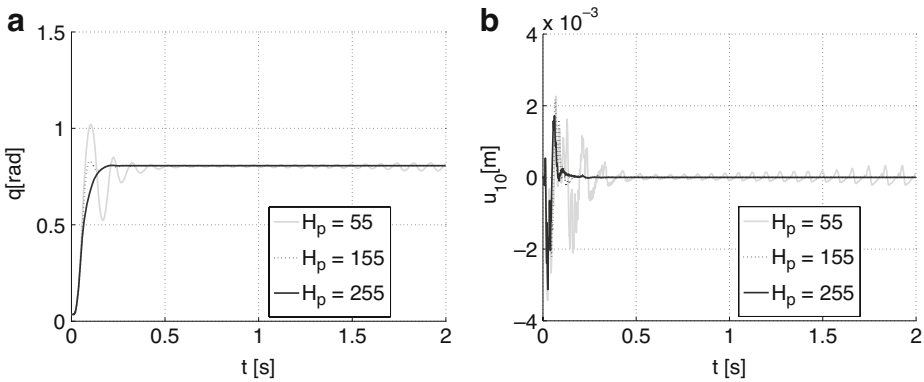

Fig. 21 Analysis of the effects of different prediction horizon H_p on a perturbed version of the plant: **a** Angular position q. **b** Elastic displacement u_{10} measured in the local reference frame

mainly the robustness of the closed-loop system. Here some results on a perturbed plant are presented, just to show that a longer prediction horizon can be used to increase the robustness of the controller. In Fig. 21 the results of a set of experimental test are presented: the original control system (with $H_p = 55$ and $H_c = 15$) is employed to control a plant with some parametric mismatches: in the model used for prediction there is a 10% overestimation of the length of the first link L_1, a 30% overestimation of the linear mass density of the links m and of the Young's modulus E, while the torque actually applied to the plant is 30% more than the desired one. It can be seen that this perturbed plant is no more stable when the prediction horizon is $H_p = 55$. By increasing this value (in Fig. 21 the results are presented for $H_p = 155$ and $H_c = 255$) stability and good performance can be obtained. It should also be noticed that increasing the prediction horizon has less effects on the increasing of the overall computational weight required by the MPC controller than the increasing of the control horizon H_c.

9 Position Control (PID): Simulation Results

Here a PID control is implemented and tested: the simulation results are used to compare the proposed MPC controller with a traditional and commonly used control technique. The target of the tuning of the PID is to move the mechanism at the same speed that can be obtained with the MPC controller. This is because the maximum amplitude of the vibration phenomena are directly proportional to the moving speed of the mechanism.

As it can be seen in Fig. 22 PID control has a very subtle effects on vibration damping in a four-link mechanism. Looking at Fig. 22 it can be seen that PID allows the mechanism to follow with high speed and no permanent error the reference trajectory, but a noticeable overshoot ($\approx 35\%$) is still present. This overshoot phenomenon can be eliminated, but at the cost of reducing the rise time of the

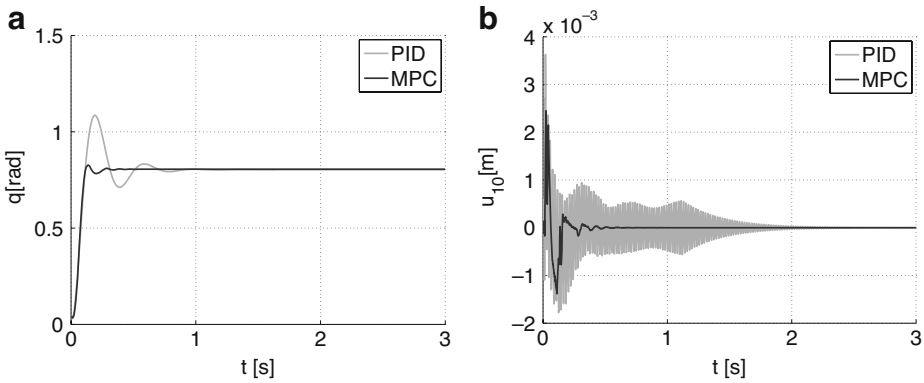

Fig. 22 Comparison of the response of the system with PID and MPC control. **a** Angular position q. **b** Elastic displacement u_{10}

Table 2 Comparison of vibration damping times and % overshoot

Controller	$\lvert\Delta u_{10}\rvert < 1mm$	$\lvert\Delta u_{10}\rvert < 0.1mm$	$\lvert\Delta u_{10}\rvert < 0.02mm$	Overshoot %
PID	244 ms	1860 ms	3215 ms	34.74
MPC @ 1 kHz	119 ms	294 ms	480 ms	2.54
MPC @ 100 Hz	140 ms	1530 ms	2645 ms	0.7

system, namely decreasing the overall speed of the mechanism. A comparison of the effective time required to keep the vibration under certain thresholds are presented in Table 2, but it also can be clearly seen from Fig. 22b that the MPC controller has a superior vibration reduction capability.

9.1 Comparison of Effective Vibration Damping

Here a comparison of the damping effects obtained with the PID control, the MPC controller with $f_c = 1kHz$ and the MPC controller with $f_c = 100Hz$ is presented. Considering the time required to keep transverse displacement inside a ± 1 mm, both MPC behave considerably better than the PID: this requires a 244 ms to respect this limit, while the two MPC need only 119 ms and 140. Then, PID takes 1.86 s to reduce vibration below 0.1 mm and 2.65 s to get under 0.02 mm, while the "slow" MPC requires respectively 1.53 s and 2.645 s. The best performances can be obtained with the MPC operating at 1 kHz: 294 ms after the reference step u_{10} is kept below 0.1 mm and after a mere 480 ms below 0.02 mm. PID has 34.74% overshoot, which can be unacceptable in some practical situations. The "fast" MPC has a mere 2.54% overshoot, meanwhile the slower MPC has even less overshoot (0.7%), but it should be pointed out that the slow MPC controller has also a slightly slower rise time than the MPC operating at 1 kHz.

10 Conclusion

A high accuracy FEM-based dynamical model of a four-bar flexible link mechanism has been presented in this paper. This model has been employed in software simulation environment to investigate the effectiveness of MPC control strategy for vibration damping in flexible closed-loop planar mechanisms. In order to implement the control system, a linearized model of the dynamic system has been developed. This linearized state-space model is capable of a high precision approximation of mechanism dynamic behavior, on both position and vibration dynamics. A constrained Model Predictive Control (MPC) system has been employed to control both the angular position and the vibrations of the mechanism. The optimal performance have been tested on the nominal plant, meanwhile a robustness analysis has been conducted by the means of exhaustive tests conducted on different perturbed plants. The performances of this control systems have been then compared to the ones that can be obtained trough a standard PID control. MPC control has proved to be very effective both for reference position tracking and vibration suppression, and has exposed a good level of robustness to uncertainties on the plant and to mismatches between the actual and the measured control variable.

References

1. Qin, S.J., Baggwell, T.A.: A survey of industrial model predictive control technology. Control Eng. Pract. **11**, 733–764 (2003)
2. Chen, X.-S., Li, Q., Fei, S.-M.: Constrained model predictive control in ball mill grinding process. Powder Technol. **186**, 31–39 (2008)
3. Perez, T., Goodwin, G.C., Tzeng, C.W.: Model predictive rudder roll stabilization control for ships. In: Proc. 5th IFAC Conf. on Manouvering and Control of Marine Craft, Aalborg, Denmark (2000)
4. Bleris, L.G., Vouzis, P.D., Arnold, M.G., Kothare, M.V.: A Co-Processor FPGA Platform for the Implementation of Real-Time Model Predictive Control American Control Conference 2006 (ACC'06), Minneapolis, Minnesota, 14–16 June 2006
5. Morari, M., Baotić, M., Borrelli, F.: Hybrid systems modeling and control. Eur. J. Control **9**, 177–127 (2003)
6. Murray, R.M., Hauser, J., Jadbabie, A., Milam, M.B., Petit, N., Dunbar, W.B., Franz, R.: Online control customization via aptimization-based control. In: Samad, T., Balas, G. (eds.) Software-Enabled Control. IEEE and Wiley, New York (2003)
7. Hassapis, G.: Implementation of model predictive control using real-time multiprocessing computer. Multiprocess. Microsyst. **27**, 327–340 (2003)
8. Ling, K.V., Yue, S.P., Maciejowski, J.: A FPGA implementation of model predictive control. In: Proceedings of American Control Conference, 14–16 June 2006
9. He, M., Chen, C., Zhang, X.: FPGA implementation of a recursive rank one updating matrix inversion algorithm for constrained MPC. Intell. Control Autom. **1**, 733–737 (2006)
10. Hassan, M., Dubay, R., Li, C., Wang, R.: Active vibration control of a flexible one-link manipulator using a multivariable predictive controller. Mechatron. **17**, 311–323 (2007)
11. Boscariol, P., Gasparetto, A., Zanotto, V.: Vibration reduction in a single-link flexible mechanism trough the synthesis of an MPC controller. In: Proc. of IEEE Int. Conf. on Mechatronics, Malaga, Spain, 14–17 April 2009
12. Gasparetto, A.: Accurate modeling of a flexible-link planar mechanism by means of a linearized model in the state-space form for design of a vibration control. J. Sound Vibr. **240**(2), 241–262 (2001)
13. Giovagnoni, M.: A numerical and experimental analysis of a chain of flexible bodies. J. Dyn. Syst. Meas. Control **113**, 73–80 (1994)
14. Gasparetto, A., Zanotto, V.: Vibration reduction in a flexible-link mechanism through synthesis of an optimal controller. Meccanica **41**, 611–622 (2006)
15. Gasparetto, A.: On the modeling of flexible-link planar mechanisms: experimental validation of an accurate dynamic model. J. Dyn. Syst. Meas. Control **126**, 365–375 (2004)
16. Trevisani, A.: Feedback control of flexible four-bar linkages: a numerical and experimental investigation. J. Sound Vibr. **268**, 947–970 (2003)
17. Caracciolo, R., Ceresole, E., Giovagnoni, M.: Control experiment of a flexible robot arm using the floating frame model. J. Robot. Mechatronics **8**, 112–121 (1996)
18. Caracciolo, R., Trevisani, A.: Simultaneous rigid-body motion and vibration control of a flexible four-bar linkage. Mech. Mach. Theory **36**(2), 221–243 (2001)
19. Caracciolo, R., Richiedei, D., Trevisani, A., Zanotto, V.: Robust mixed-norm position and vibration control of flexible link mechanisms. Mechatron. **15**, 767–791 (2005)
20. Franklin, F.G., Powell, J.D., Workman, M.L.: Digital Control of Dynamic Systems, 2nd ed. Addison Wesley, Reading (1990)
21. Maciejowski, J.M.: Predictive Control with Constraints. Prentice Hall, Englewood Cliffs (2002)
22. Ghahrmani, N.O., Towhidkhah, F.: Constrained incremental predictive controller design for a flexible joint robot. ISA Trans. **48**, 321–326 (2009)